Original Article

Sound transmission through sandwich plate with hourglass lattice truss core

Zhen-Kun Guo[1,2], Guobiao Hu[2], Vladislav Sorokin[2], Yi Yang[2] and Lihua Tang[2] (iD)

Abstract

This article is devoted to investigating sound insulation performance of a simply supported sandwich plate with an hourglass lattice core. The governing equations of lattice core sandwich plate are established using the Reissner sandwich plate theory. The solutions are derived using Fourier series expansion. The developed model is verified through the comparison with the results of the models from the existing literature, as well as finite element method (FEM). The effects of various structural and material parameters, the incident angle, and azimuth angle of the incident sound on sound insulation characteristics are investigated. It is demonstrated that the sandwich plate with the hourglass lattice core can outperform that with the traditional lattice cores. This work provides useful guidelines for the design of lightweight lattice sandwich structures in the application of sound insulation.

Keywords

Sandwich plate, hourglass lattice core, sound transmission loss, sound insulation, sound trough

[1]College of Mechanical Engineering, Beijing University of Technology, Beijing, China
[2]Department of Mechanical Engineering, University of Auckland, Auckland, New Zealand

Corresponding author:
Lihua Tang, Department of Mechanical Engineering, University of Auckland, 20 Symonds Street, Auckland 1010, New Zealand.
Email: l.tang@auckland.ac.nz

Introduction

Lightweight sandwich structures have attracted lots of research interest due to the outstanding characteristics such as low density but high strength [1], shock resistance [2], sound absorption [3–5], electromagnetic wave absorption [6], and efficient heat isolation [7,8]. A sandwich structure could be regarded as a multi-layered structure consisting of two or more face sheets with high strength and stiffness separated by one or more soft cores with low density. The studies on sandwich structures have been predominantly concentrated on the static properties [9–12] and dynamic properties [13–17]. Sound propagation properties of sandwich structures are also important in their applications for sound insulation.

In the past decade, sound insulation characteristics of the sandwich structures have been investigated using various methods. The statistical energy method [18–22] assumes that vibration modes are intensive in high frequency ranges, thus is strongly limited for high frequency vibration and acoustic analysis. The space-harmonics method has also been extensively exploited for the vibration and sound radiation analysis of periodic structures. Lee and Kim [23,24] firstly studied the sound insulation of a cylindrical shell and plate reinforced by periodically arranged stiffeners, and derived the governing equations through expanding the vibro-acoustic response into space harmonics. Similarly, researchers applied the space-harmonics method to study the sound transmission loss (STL) of two-dimensional and three-dimensional sandwich plates [25–28]. However, this approach is mainly used for analyzing the dynamics of infinite periodic structures. The transfer matrix method was also used for calculating the STL through the infinitely extended construction which was made up of two solid plates and a series of layers of porous materials [29].

Finite element method (FEM) and boundary element method, as numerical methods, are also widely used in acoustic analysis since they can in principle be applied for any complicated structures [30–32]. However, the complexity of the structure geometry inevitably increases the computational expense and the accumulative error often becomes significant in high frequency ranges. For the finite sandwich structures, the vibro-acoustic performance has been investigated theoretically [33,34] using the modal function and Fourier series expansion, as well as experimentally [35,36]. However, most of them did not clearly explain the generation mechanism of sound troughs and the disappearance of sound troughs for certain azimuth angles under the oblique incident sound wave.

Although the static mechanical properties of the sandwich plate with hourglass core have been extensively investigated [37–39], studies on its dynamic properties are quite rare [17] in the literature. And the sound insulation performance of simply supported sandwich plate with different lattice truss cores under both oblique sound wave and diffuse sound field have not been fully explored. Inspired by the aforementioned research, this work proposes a study on vibration and STL properties of the sandwich plate with an hourglass lattice core and attempts to fill this gap. First, the hourglass lattice core sandwich structure

model is established using the Reissner sandwich plate theory. The natural frequencies are analytically determined and validated by existing literature and FEM. The STL is calculated by Fourier series expansion and validated by FEM. Subsequently, the sound insulation performance of sandwich plates with hourglass, tetrahedral and pyramidal lattice cores are compared and discussed. Finally, the effects of various parameters on vibration and sound insulation characteristics of the hourglass lattice core sandwich plate are analyzed.

Theoretical modeling

Model formulation

Figure 1(a) shows the hourglass lattice truss core designed by Feng et al. [37,38] for being used in sandwich structures. Though it is similar to the double-layer pyramidal truss lattice, its shear strength, compressive properties, and bending failure loading capacity have been proved more excellent than the traditional pyramidal
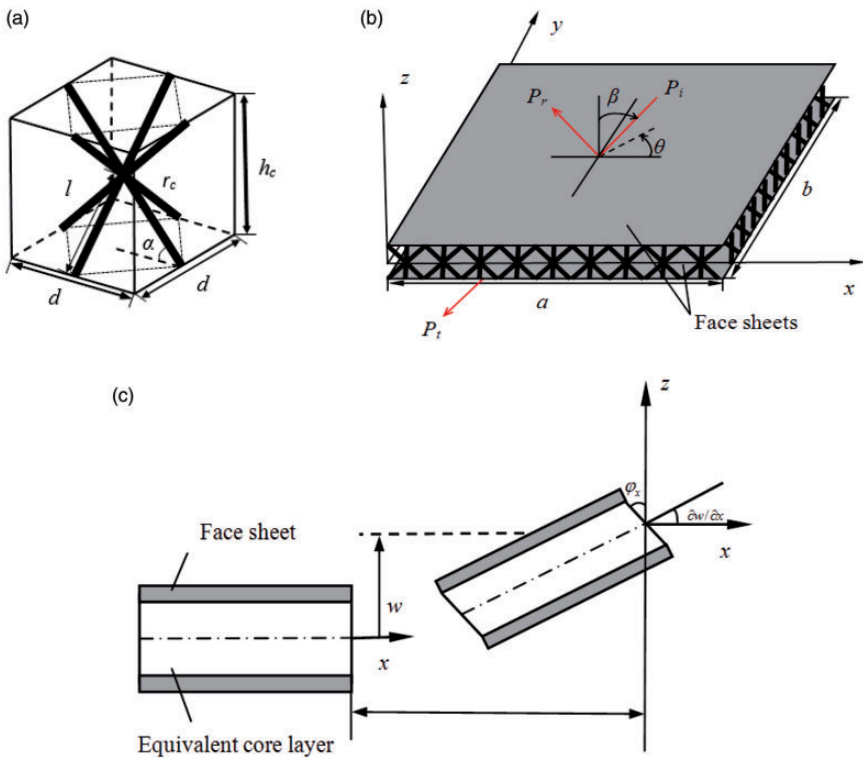

Figure 1. (a) Hourglass core, (b) sandwich plate subjected to an incident sound wave, and (c) deformation diagram of a differential element of the sandwich plate.

one. The length, height, and radius of the rod of the lattice core are l, h_c, and r_c, respectively. The span of one unit is d, and the inclination angle between the rod and sheets is α. The relationships of the main parameters of the hourglass lattice truss core can be obtained as $l = h_c/\sin\alpha$, $d = h_c/\tan\alpha$. Figure 1(b) shows the sandwich plate under sound pressure. The sandwich plate consists of top and bottom face sheets and hourglass lattice core. The x, y, and z directions correspond to the length, width, and height of the sandwich plate, respectively. The length, width, and thickness of the face sheets are a, b, and h_f, respectively. The incident, reflected, and transmitted sound waves are denoted by P_i, P_r, and P_t, respectively. β and θ represent the incident and azimuth angles of incident sound wave, respectively. Figure 1(c) shows the deformation of a differential element of the sandwich plate with length dx and width dy. The rotating angles of face sheets and core layer are $\partial w/\partial x$ and φ_x around the y axis, respectively.

Considering the form of sandwich structure and its boundary conditions as well as the acoustic characteristics of the sound field, the Reissner theory is utilized for formulating the analytical model [40], which considers shear strains of the core on basis of classical plate theory. The total moments and shear forces can be expressed as

$$M_x = -D\left(\frac{\partial\varphi_x}{\partial x} + v_f\frac{\partial\varphi_y}{\partial y}\right), \quad M_y = -D\left(v_f\frac{\partial\varphi_x}{\partial x} + \frac{\partial\varphi_y}{\partial y}\right),$$

$$M_{xy} = -\frac{1}{2}D(1 - v_f)\left(\frac{\partial\varphi_x}{\partial y} + \frac{\partial\varphi_y}{\partial x}\right), \quad Q_x = C\left(\frac{\partial w}{\partial x} - \varphi_x\right), \quad Q_y = C\left(\frac{\partial w}{\partial y} - \varphi_y\right)$$

$$(1)$$

where w is the transverse displacement of the sandwich plate. $D = \frac{E_f(h_c+h_f)^2 h_f}{2(1-v_f^2)}$ is the effective bending stiffness of the hourglass lattice core sandwich plate, in which E_f and v_f represent the Young's modulus and Poisson's ratio of the face sheets, respectively. $C = \frac{2\pi r_c^2 E_s h_c \sin\alpha}{l^2}$ is the equivalent shear stiffness of core layer [37,41], in which E_s denotes the Young's modulus of rods. Generally, for the core layer, the bending stiffness can be neglected and only the shear deformation is considered for certain structural sizes of the lattice sandwich plates [42,43], which will be discussed in "Parametric study on vibro-acoustic performance" section. By using the Reissner sandwich plate theory, the equilibrium equations are written as

$$\frac{\partial M_x}{\partial x} + \frac{\partial M_{xy}}{\partial y} - Q_x = 0, \quad \frac{\partial M_{xy}}{\partial x} + \frac{\partial M_y}{\partial y} - Q_y = 0, \quad \frac{\partial Q_x}{\partial x} + \frac{\partial Q_y}{\partial y} + q - \rho_s\frac{\partial^2 w}{\partial t^2} = 0$$

$$(2)$$

where q is the external load applied on the sandwich plate. $\rho_s = h_c\rho_c + 2h_f\rho_f$ is the equivalent mass density per unit area of the sandwich plate, in which ρ_f is

the mass density of sheets. $\rho_c = \frac{4\pi r_c^2 \rho_r}{l^2 \sin\alpha \cos^2\alpha}$ is the equivalent density of core layer and ρ_r denotes the density of rods. Based on the in-unison vibration concept of modal motions, a technique has been proved efficient to reduce the dimension of the continuous systems, where functional relations between different degrees of freedom exist [44]. Further, according to Guo et al. [45], φ_x and φ_y have certain linear relationship with $\partial w/\partial x$ and $\partial w/\partial y$ corresponding to each vibration mode, which indicates that they are not completely independent. This implies that the status of the sandwich plate at any point could actually be described by using two functions instead of three. By introducing two independent functions ψ and f, the rotation angles and the transverse displacement are expressed as

$$\varphi_x = \frac{\partial \psi}{\partial x} + \frac{\partial f}{\partial y}, \quad \varphi_y = \frac{\partial \psi}{\partial y} - \frac{\partial f}{\partial x}, \quad w = \psi - \frac{D}{C}\nabla^2\psi \tag{3}$$

By substituting equation (3) into equation (1) and then combining the resultants with equation (2), the governing equations of sandwich plate are obtained as

$$D\nabla^2\nabla^2\psi + \rho_s \frac{\partial^2}{\partial t^2}\left(\psi - \frac{D}{C}\nabla^2\psi\right) = q, \quad \frac{D}{2}(1 - v_f)\nabla^2 f - Cf = 0 \tag{4}$$

Considering that the sandwich plate is simply supported, we can write the boundary conditions as [46]

$$\begin{aligned} w = 0, \quad M_x = 0, \quad \varphi_y = 0, \quad \text{for } x = 0 \text{ and } a \\ w = 0, \quad M_y = 0, \quad \varphi_x = 0, \quad \text{for } y = 0 \text{ and } b \end{aligned} \tag{5}$$

where the reason for $\varphi_y = 0$ or $\varphi_x = 0$ is given in Appendix 1.

Substituting equations (1) and (3) into equation (5) yields

$$\begin{aligned} \psi = 0, \quad \frac{\partial^2\psi}{\partial x^2} = 0, \quad \frac{\partial^4\psi}{\partial x^4} = 0, \quad \frac{\partial f}{\partial x} = 0, \quad \text{for } x = 0 \text{ and } a \\ \psi = 0, \quad \frac{\partial^2\psi}{\partial y^2} = 0, \quad \frac{\partial^4\psi}{\partial y^4} = 0, \quad \frac{\partial f}{\partial y} = 0, \quad \text{for } y = 0 \text{ and } b \end{aligned} \tag{6}$$

For the simply supported sandwich plate, it is deduced that $f \equiv 0$ from equations (3), (5), and (6). The detailed derivation procedures are provided in Appendix 2. Omitting the applied load, the governing equation is written as

$$D\nabla^2\nabla^2\psi + \rho_s \frac{\partial^2}{\partial t^2}\left(\psi - \frac{D}{C}\nabla^2\psi\right) = 0 \tag{7}$$

The deformation of freely vibrating sandwich plate that satisfies the boundary conditions (i.e., equation (6)) is given as

$$\psi = A_{mn}\sin\frac{m\pi x}{a}\sin\frac{n\pi y}{b}e^{j\omega_{mn}t} \tag{8}$$

where $j = \sqrt{-1}$ is the imaginary unit, A_{mn} is the amplitude of ψ, and ω_{mn} denotes the circular frequency of freely vibrating sandwich plate which is obtained by substituting equation (8) into equation (7)

$$\omega_{mn}^2 = \frac{D\pi^4}{\rho_s a^4}\frac{(m^2 + \lambda^2 n^2)^2}{1 + k^2(m^2 + \lambda^2 n^2)}, \quad (m, n = 1, 2, 3, \ldots) \tag{9}$$

where m and n represent the mode numbers, $k = \frac{\pi}{a}\sqrt{\frac{D}{C}}$ and $\lambda = \frac{a}{b}$. Therefore, the natural frequencies are expressed as

$$f_{mn} = \frac{\pi}{2a^2}\sqrt{\frac{D}{\rho_s}\frac{(m^2 + \lambda^2 n^2)^2}{1 + k^2(m^2 + \lambda^2 n^2)}}, \quad (m, n = 1, 2, 3, \ldots) \tag{10}$$

With a harmonic travelling plane wave obliquely incident on the top face sheet (as shown in Figure 1(b)), the incident pressure wave is given as

$$P_i(x, y, z, t) = P_{i0}e^{j(\omega t - k_x x - k_y y - k_z z)} \tag{11}$$

where P_{i0} and ω represent amplitude and circular frequency of the incident wave, respectively. k_x, k_y, and k_z are the components of wave number along the x-, y- and z-directions and they are expressed as

$$k_x = k_0\sin\beta\cos\theta, \quad k_y = k_0\sin\beta\sin\theta, \quad k_x = k_0\cos\theta \tag{12}$$

where $k_0 = \frac{\omega}{c}$ denotes wave number of the sound waves in air, and c denotes the sound speed. The reflected sound pressure of the top face sheet is given as [47]

$$P_r(x, y, z, t) = \sum_{m=1}^{\infty}\sum_{n=1}^{\infty}W_{mn}P_{rmn}e^{j(\omega t + k_z z)} \tag{13}$$

where $W_{mn} = \sin\frac{m\pi x}{a}\sin\frac{n\pi y}{b}$ is the shape function of sandwich plate, P_{rmn} are modal amplitudes of the reflected sound pressure. Similarly, the transmitted sound pressure is expressed as [47]

$$P_t(x, y, z, t) = \sum_{m=1}^{\infty}\sum_{n=1}^{\infty}W_{mn}P_{tmn}e^{j(\omega t - k_z z)} \tag{14}$$

where P_{tmn} are modal amplitudes of the transmitted pressure wave. The governing equation of the sandwich plate under the excitation of the combined sound pressure (i.e., incident, reflected and transmitted sound pressures) can be obtained as

$$
\begin{aligned}
D\nabla^2\nabla^2\psi + \rho_s\frac{\partial^2}{\partial t^2}\left(\psi - \frac{D}{C}\nabla^2\psi\right) \\
= p_i\left(x, y, \frac{h_c + 2h_f}{2}, t\right) + p_r\left(x, y, \frac{h_c + 2h_f}{2}, t\right) - p_t\left(x, y, -\frac{h_c + 2h_f}{2}, t\right)
\end{aligned}
\tag{15}
$$

By using the Fourier Series expansion, the incident sound pressure can be expressed as

$$
P_{i0}e^{j(\omega t - k_x x - k_y y - k_z z)} = \sum_{m=1}^{\infty}\sum_{n=1}^{\infty}W_{mn}P_{imn}e^{j(\omega t - k_z z)}
\tag{16}
$$

and the modal amplitudes of the incident pressure wave can be obtained as

$$
P_{imn} = \frac{4}{ab}\int_0^a\int_0^b P_{i0}e^{j(-k_x x - k_y y)}W_{mn}\mathrm{d}x\mathrm{d}y
\tag{17}
$$

After the integral calculation, P_{imn} is expressed as follows

$$
P_{imn} = \frac{4mn\pi^2 P_{i0}(e^{-jk_x a}\cos m\pi - 1)(e^{-jk_y b}\cos n\pi - 1)}{[(k_x a)^2 - (m\pi)^2][(k_y b)^2 - (n\pi)^2]}
\tag{18}
$$

At the interfaces between the air and face sheets, the continuity conditions of acoustic and elastic velocities normal to the face sheets require

$$
\begin{aligned}
\frac{\partial(P_i + P_r)}{\partial z} = \rho_0\omega^2 w, \quad \text{for } z = \frac{h_c + 2h_f}{2}, \\
\frac{\partial P_t}{\partial z} = \rho_0\omega^2 w, \quad \text{for } z = -\frac{h_c + 2h_f}{2}
\end{aligned}
\tag{19}
$$

where ρ_0 denotes the density of air.

For the forced vibration of sandwich plate, dynamic response is obtained by the superposition of mode shapes

$$
\psi = \sum_{m=1}^{\infty}\sum_{n=1}^{\infty}A_{mn}W_{mn}e^{j\omega t}
\tag{20}
$$

Substituting equations (11), (13), (14), and (16) into equation (19), and combining with equations (3) and (20), the relationships between P_{rmn}, P_{tmn}, and A_{mn} can be obtained

$$P_{rmn} = \frac{A_{mn}(B_{mn}D/C + 1)\rho_0\omega^2}{jk_z e^{-jk_z(h_c/2+h_f)}} + P_{imn}e^{jk_z(h_c+2h_f)} \tag{21}$$

$$P_{tmn} = \frac{A_{mn}(B_{mn}D/C + 1)\rho_0\omega^2}{-jk_z e^{-jk_z(h_c/2+h_f)}} \tag{22}$$

where $B_{mn} = \left(\frac{m\pi}{a}\right)^2 + \left(\frac{n\pi}{b}\right)^2$. Substituting equations (21) and (22) into equations (13) and (14), and then combining with equations (20) and (15), the coefficient A_{mn} can be obtained as

$$A_{mn} = \frac{2P_{imn}e^{jk_z(h_c/2+h_f)}}{DB_{mn}^2 - \omega^2\left(\rho_s - \frac{2j\rho_0}{k_z}\right)\left(\frac{D}{C}B_{mn} + 1\right)} \tag{23}$$

Substituting equation (23) into equation (22), P_{tmn} can be expressed as

$$P_{tmn} = \frac{j\rho_0\omega^2\left(\frac{D}{C}B_{mn} + 1\right)e^{jk_z(h_c/2+h_f)}}{k_z}A_{mn} \tag{24}$$

The transmission coefficient under an oblique incident sound wave is defined as

$$\tau[(\beta, \theta)] = W_i/W_t \tag{25}$$

in which W_i and W_t are the incident and transmitted sound power, respectively, and they are expressed as

$$W_i = \frac{1}{2}\text{Re}\int\int_A P_i \cdot v_i^* dA \tag{26}$$

$$W_t = \frac{1}{2}\text{Re}\int\int_A P_t \cdot v_t^* dA \tag{27}$$

where $v_i = P_i/(\rho_0 c)$ and $v_t = P_t/(\rho_0 c)$ are the acoustic particle velocities on the incident and transmitted sides, respectively. The superscript star "*" means the complex conjugate. Since resultant power intensity of a multi-frequency wave is

the linear superposition of the power intensities of each frequency component, one obtains

$$\frac{W_i}{W_t} = \frac{\sum_{m=1}^{\infty}\sum_{n=1}^{\infty}|P_{imn}|^2}{\sum_{m=1}^{\infty}\sum_{n=1}^{\infty}|P_{tmn}|^2} \tag{28}$$

The transmission coefficient under the diffuse incident field is given as [34]

$$\tau_d = \frac{\int_0^{2\pi}\int_0^{\pi/2}\tau(\beta,\theta)\sin(\beta)\cos(\beta)\mathrm{d}\beta\mathrm{d}\theta}{\int_0^{2\pi}\int_0^{\pi/2}\sin(\beta)\cos(\beta)\mathrm{d}\beta\mathrm{d}\theta} \tag{29}$$

Based on equations (25) and (29), the STL for the sandwich plate under an oblique incident sound wave and diffuse incident field can be calculated by [32]

$$STL = \begin{cases} 10\lg[\tau(\beta,\theta)] \\ 10\lg\tau_d \end{cases} \tag{30}$$

Model validation

The natural frequencies of an example pyramidal lattice core sandwich plate model from the literature [46] are calculated by using the method presented in the previous section, in which the core layer and face sheets are all made of steel. The dimensions and material parameters used in the calculation are: $\rho_f = 7800\,\mathrm{kg/m^3}$, $E_f = 210\,\mathrm{GPa}$, $\nu = 0.3$, $a = 1.06\,\mathrm{m}$, $b = 1.06\,\mathrm{m}$, $r_c = 3 \times 10^{-3}\,\mathrm{m}$, $h_f = 2.5 \times 10^{-3}\,\mathrm{m}$, $h_c = 0.03\,\mathrm{m}$, and $d = 0.0424\,\mathrm{m}$. The results are listed in Table 1 and compared with the published literature [46,48, 49]. The relative errors are acceptable and it is noted that the results calculated by the analytical method are a bit higher because

Table 1. Natural frequencies of the pyramidal lattice core sandwich plate by different methods.

Modes (m, n)	(1, 1)	(1, 2), (2,1)	(2, 2)	(1, 3), (3, 1)	(2, 3), (3, 2)
Ref. [46]	203.76 Hz	445.10 Hz	640.37 Hz	752.51 Hz	903.89 Hz
Ref. [48]	204.93 Hz	451.02 Hz	652.01 Hz	769.27 Hz	927.07 Hz
Ref. [49]	193.88 Hz	448.95 Hz	646.92 Hz	791.90 Hz	945.07 Hz
Present method	206.63 Hz	458.04 Hz	665.20 Hz	786.59 Hz	950.41 Hz

the Reissner plate theory does not take into account the influence of rotary inertia which was taken into account in the references.

To verify the effectiveness of the presented model in-depth, FEM is used to calculate the frequencies of the hourglass lattice truss core sandwich plate. Material and geometric parameters for the sandwich structure composed of steel are listed in Table 2. The length and width of the hourglass core sandwich plate are set to be the lengths of 30 and 25 unit cells, respectively.

The natural frequencies of simply supported sandwich plate calculated by the analytical method and FEM are presented in Table 3. The model in Figure 2 is built by commercial software ANSYS, in which the face sheets are emulated by SHELL181 element and the lattice truss core is emulated by BEAM189 element. After generating the mesh, the coincident nodes of the shell and beam elements are merged to ensure the sheets and rods are consolidated at top and bottom inter-faces. It is noteworthy that the top and bottom face sheets section offset should be respectively bottom-plane and top-plane to keep the bending stiffness of the sandwich plate accuracy. A good agreement could be observed between the results from the analytical model and FEM.

Further, the results of modal analysis for the simply supported sandwich plate from ANSYS are imported into the commercial software Virtual Lab for calculating the STL. The reverberation and anechoic chambers are simulated by two

Table 2. Material and geometric parameters of the hourglass lattice core sandwich plate.

E_f, E_s (GPa)	υ	ρ_f, ρ_r (kg/m^3)	h_f (mm)	h_c (mm)	r_c (mm)	α (°)	a (mm)	b (mm)
210	0.3	7930	1	15	1	45	450	375

Table 3. Natural frequencies (Hz) of the hourglass lattice core sandwich plate.

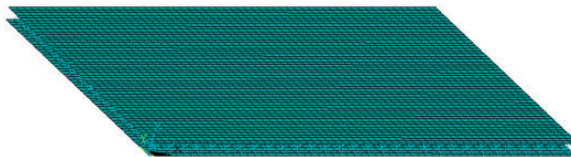| Modes (m, n)	(1, 1)	(2,1)	(1, 2)	(2,2)	(3, 1)
Present model	615.53 Hz	1298.04 Hz	1576.88 Hz	2170.07 Hz	2297.57 Hz
ANSYS	615.06 Hz	1247.20 Hz	1512.00 Hz	2037.40 Hz	2128.80 Hz
Relative error	0.7%	3.9%	4.1%	6.1%	7.3%

Figure 2. Finite element model of the hourglass lattice core sandwich plate developed with ANSYS.

rectangle acoustic meshes established on the two sides of the sandwich plate as shown in Figure 3. The air density is 1.29 kg/m³ and the sound velocity is 340 m/s. The outer surfaces of the two acoustic meshes utilize the automatically matched layer. The top and bottom face sheets are coupled with the inner surfaces of reverberation and anechoic chambers, respectively. In order to calculate the STL under the oblique incident sound wave and diffuse incident field, the acoustic sources are respectively set to 1 plane wave and 12 plane waves, in which the former is incident on the sandwich plate with an incident angle $\pi/6$ and azimuth angle $\pi/4$. Finally, the STL of sandwich plate can be calculated by modal super-position vibro-acoustics response analysis. The comparison of the STL calculated by analytical method (i.e., equation (30)) and FEM under oblique sound wave and diffuse sound field are shown in Figure 4, respectively. It is observed that the amplitude and overall tendency of STL of the numerical results by FEM agree well with analytical model, while the sound troughs in analytical model move to higher frequencies than those from FEM as the frequency of sound wave increases, due to the fact that the Reissner plate theory does not take into account the rotary inertia. Because the STL under oblique sound wave shows similar tendency to that of diffuse sound field, the following studies will investigate the characteristic of STL of sandwich plate under oblique sound wave.

Model convergence

In the derivation of the STL, the dynamic response of the sandwich plate is approximated by the superposition of modal contributions. The sound pressures are also expanded in terms of the plate mode shape functions. It can be seen from
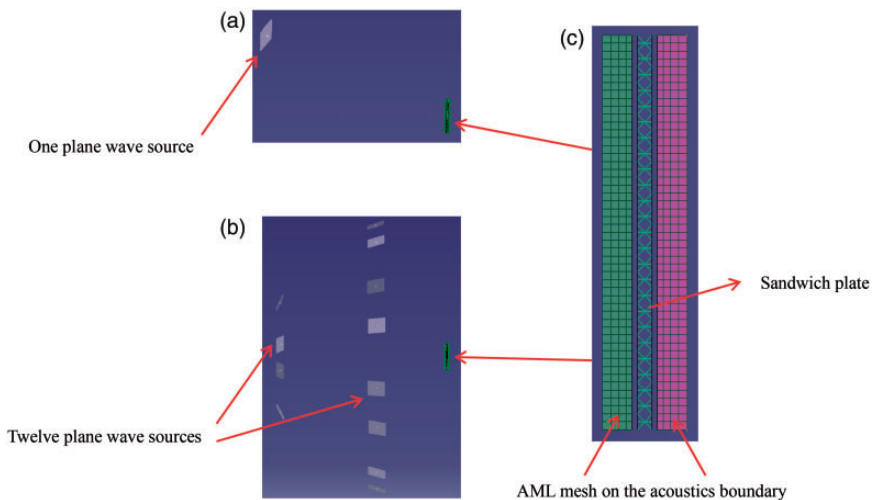

Figure 3. The acoustic vibration coupled FEM model for STL under 1 plane wave source and 12 plane wave sources.
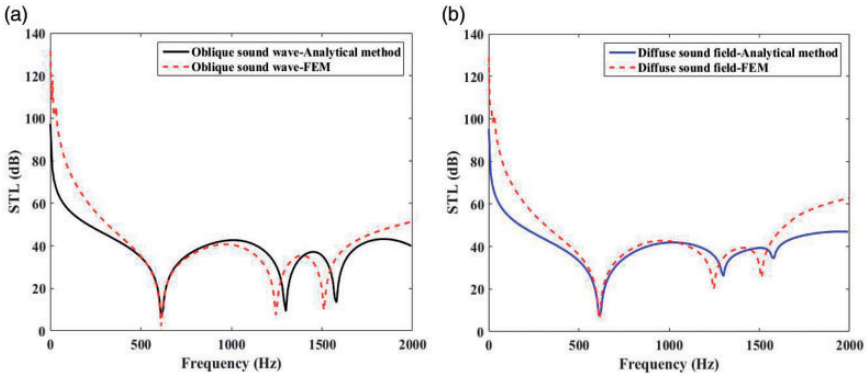
Figure 4. Comparison of STL calculated by analytical method and FEM under (a) oblique sound wave with incident angle $\beta = \pi/6$ and azimuth angle $\theta = \pi/4$ and (b) diffuse sound field.

equation (28) that the derived STL expression also includes the superposition of a series of the mode shape functions of the sandwich plate. The employment of the modal superposition method significantly reduces the complexity of the problem but the accuracy of the final result depends on the number of modes that are involved in calculation. Therefore, a simple case study is given to determine the number of modes required to ensure convergence.

Normally, for a specific frequency, if the STL result converges, then the model convergence in the entire range below that frequency can be guaranteed by using the same number of modes in calculation. To verify convergence of the theoretical model, the sound insulation at 5000 Hz is calculated with varying number of modes included. By regarding the STL value calculated using 200 modes (i.e., $m = n = 200$) as converged, the evolution of the relative error of the STL value with the variation of the number of modes being used in the calculation is shown in Figure 5. It is noted that the result can already be deemed as converged when m/n is larger than 100. Therefore, in consideration of the balance between the computation cost and accuracy, m and n are both set to be 100 in the following case studies.

Sound trough generation mechanism

From the STL spectrum of the hourglass lattice core sandwich plate presented in Figure 4(a), it is observed that when the incident angle is $\pi/6$ and the azimuth angle is $\pi/4$, in the frequency range from 0 to 2000 Hz, there exist three sound troughs which corresponds to the first three natural frequencies. This is because when the frequencies of incident sound waves match the natural frequencies of sandwich plate, resonance phenomenon occurs in the sandwich plate, which leads to the generation of an intensive structure-borne sound (i.e., the transmitted sound)
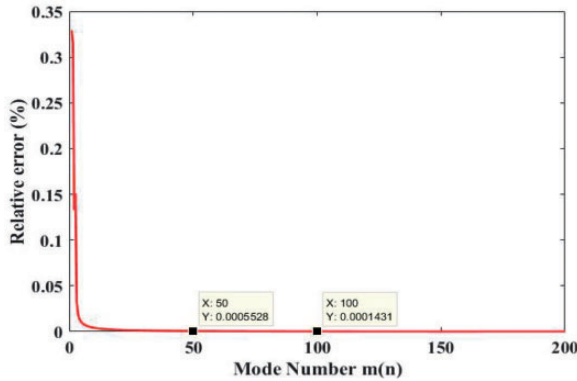
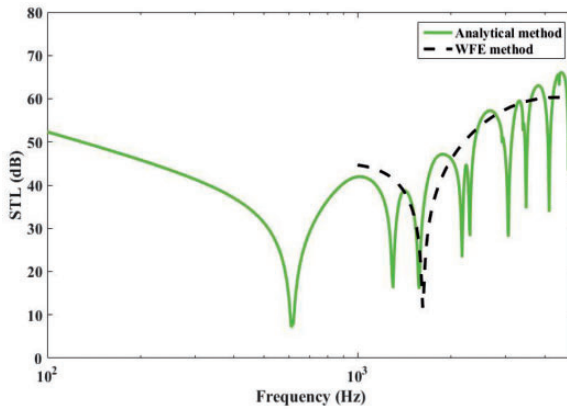**Figure 5.** The convergence of STL for the sandwich plate with hourglass lattice core.

Figure 6. Comparison of STL for the finite and infinite sandwich plates with hourglass core.

and minimum STL [35]. Consequently, a great portion of the sound energy penetrates the sandwich plate and the sound troughs form in the STL spectrum.

Comparison between analytical and WFE methods

Figure 6 depicts the STL for an incident sound wave with $(\beta, \theta) = (\pi/3, \pi/6)$ by using the analytical method presented in this work and the wave finite element (WFE) method [32]. It is worth mentioning that the analytical method calculates a finite sandwich plate with simply supported boundary conditions, while the WFE method calculates an infinite sandwich plate. The troughs in the solid curve are induced by the structural resonances while the trough on the dashed line is due to coincidence (1600 Hz). It is found that at high frequencies (above
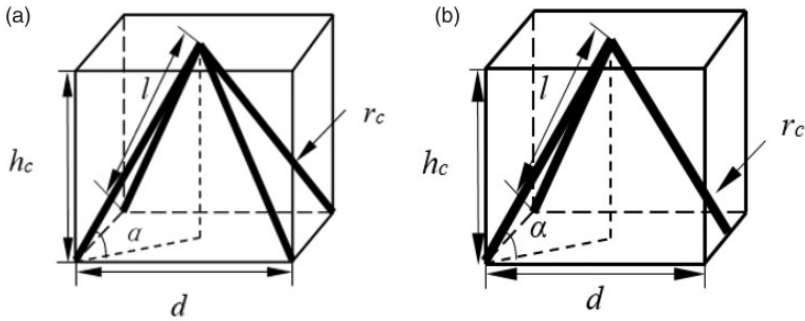
Figure 7. (a) Pyramidal lattice core, (b) tetrahedral lattice core.

1000 Hz), a good agreement on STL can be observed except for the troughs due to resonance frequencies. Therefore, this also indirectly confirms the effectiveness of present model.

Comparison of different lattice cores

It has been reported that some mechanical properties of the hourglass lattice core sandwich plate are superior to those of the traditional pyramidal one [37,38]. Therefore, it is inspired to conduct a study to compare them in terms of their dynamic properties as well. Figure 7 shows the schematics of the pyramidal and tetrahedral lattice cores.

The entire weight, structural, and material parameters of the lattice unit and sandwich plate for the pyramidal and tetrahedral cores are determined based on the hourglass lattice core plate according to the rule of weight equality. It is assumed that the length and width of the two different core sandwich plates, the span and height of a lattice unit are the same as those of hourglass core sandwich plate. Only the radius of rods is tunable and other parameters are kept constant to ensure a fair comparison among the three types of sandwich plates. The radii of rods in the pyramidal and tetrahedral lattice cores are obtained to be 1.075 mm and 1.346 mm according to the rule of weight equality, respectively.

The sound insulation performance of sandwich plates with pyramidal, tetrahedral, and hourglass lattice cores under diffuse sound field are compared in Figure 8. It can be found that most of the sound troughs of the sandwich plate with hourglass core move to higher frequencies as compared to the other two sandwich plates in the high frequency range, because the equivalent shear modulus of hourglass lattice core is higher than those of the other two counterparts (2.07, 1.84, and 1.77 GPa for the hourglass, pyramidal, and tetrahedral lattice cores, respectively). In addition, the sandwich plate with hourglass core exhibits larger peaks and smaller troughs, which indicates a better sound insulation. By contrast, the tetrahedral one shows the worst sound insulation. From this perspective, the
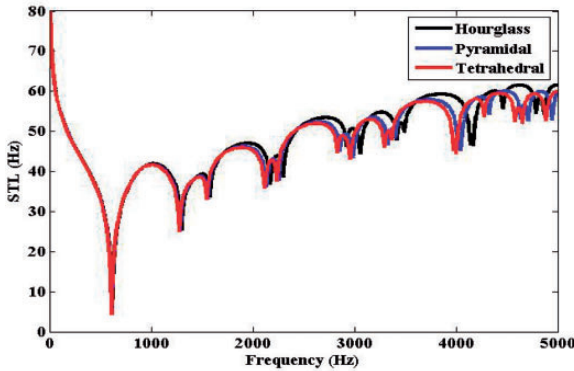
Figure 8. Comparison of STL for sandwich plates with three different lattice truss cores under diffuse sound field.

sandwich plate with hourglass lattice core deserves further investigation on its vibration and acoustic performance.

Parametric study on vibro-acoustic performance

Based on the established analytical model, effects of the geometric and material parameters on the vibro-acoustic performance of the sandwich plate with hourglass lattice core are analyzed. Recall that the contribution in the effective bending stiffness of the sandwich plate from core layer is neglected in the modeling. In order to confirm this hypothesis, a supplementary study is provided in Appendix 3 to demonstrate that when the structural parameters change within certain ranges, the sandwich core indeed has only negligible contribution to the total effective bending stiffness D of the sandwich structure.

Effect of geometric parameters

The top and bottom face sheets of the sandwich plate are joined by hourglass lattice truss core, which implies that the height of the lattice core is just the internal distance between the two sheets. Changing the height of the lattice core is equivalent to changing the inclination angle and length of rods on the premise of keeping other parameters constant. It can be speculated that the equivalent stiffness, shear stiffness, and density of the sandwich structure will change accordingly, as well as the vibro-acoustic performance.

Effect of the height of hourglass lattice core (i.e., h_c) on first four natural frequencies of the sandwich plate is demonstrated in Figure 9 where h_c ranges from 7 to 15 mm. It is observed that with the increase of h_c, all the natural frequencies show an increasing trend and the rate of increase declines gradually, because the bending and shear stiffness of the sandwich plate increase correspondingly and
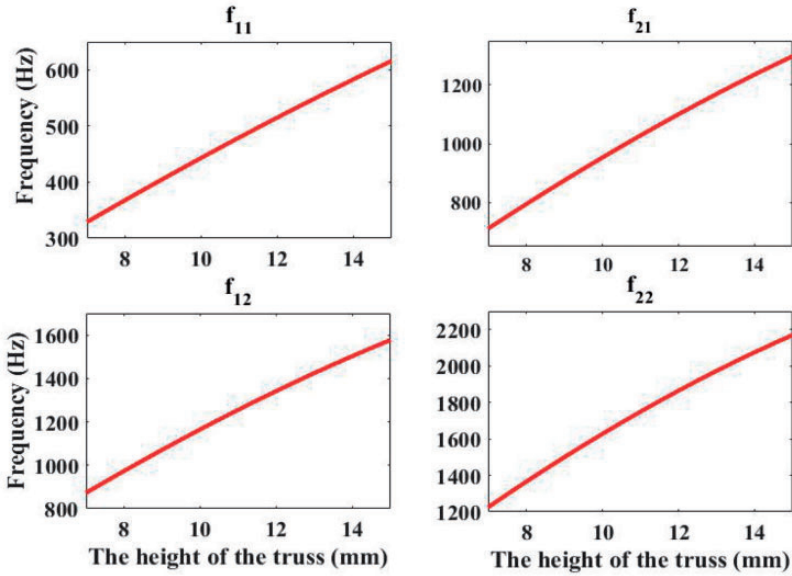
Figure 9. Effect of the height of the hourglass lattice core on the first four natural frequencies.
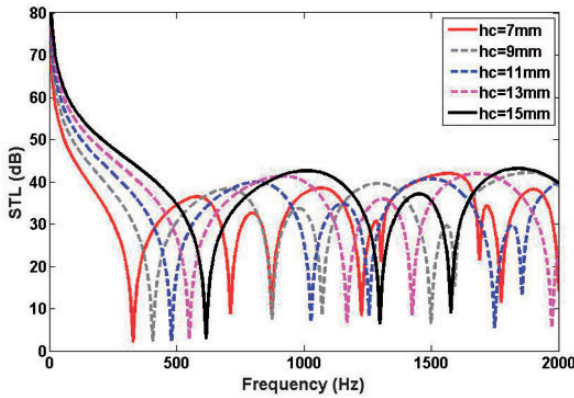

Figure 10. Effect of the height of the hourglass lattice core on STL of the sandwich plate.

they are dominant to the increasing mass. Hence, the first four natural frequencies of the sandwich plate can be tuned by changing h_c.

Figure 10 shows the STL of the sandwich plate with different h_c when the incident angle $\beta = \pi/6$ and the azimuth angle $\theta = \pi/4$. It is noted that with the increase of h_c, all the sound troughs move to the higher frequencies and the sound peaks become larger, leading to the improvement of the STL, which
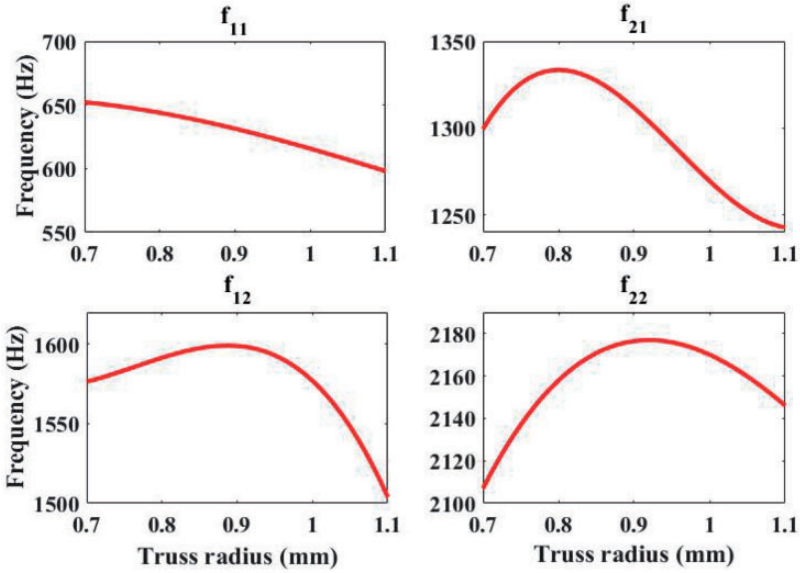
Figure 11. Effect of the rod radius on the first four natural frequencies.

is because the increased height of the core layer results in a larger core mass and air cavity thickness to improve the sound insulation [33]. Therefore, it can be concluded that it is feasible to achieve desirable STL in specific frequency ranges by controlling h_c.

The rod radius is an important structural parameter which affects the equivalent shear stiffness and density of hourglass lattice core, as well as the sound insulation performance of the sandwich plate. Figure 11 reveals its effect on the first four natural frequencies. Here, all other parameters are kept constant except for the rod radius. With the increase in rod radius, the first natural frequency declines, while the others first increase and then decrease with lower order modes having lower turning points, and the lower the frequency order results in a lower value of turning point beyond which the frequency falls. This shows a similar trend to that reported in Guo et al. [49]. This is the result of the counterbalance effect between the mass and stiffness: the higher mass brings lower frequency and the higher stiffness gives rise to higher frequency. In a word, the rod radius has different influences on different order of natural frequencies. Therefore, the sandwich plate with hourglass lattice core could obtain resonances at different frequencies by designing the radius of the rods.

Figure 12 shows the effect of the rod radius on the STL of the sandwich plate with hourglass lattice core when the incident angle $\beta = \pi/6$ and the azimuth angle $\theta = \pi/4$. It is indicated in the figure that with the increase in radius, all the sound troughs slightly move to lower frequencies. In addition, in the frequency range after first sound trough, it can be noted that the larger the rod radius is, the better
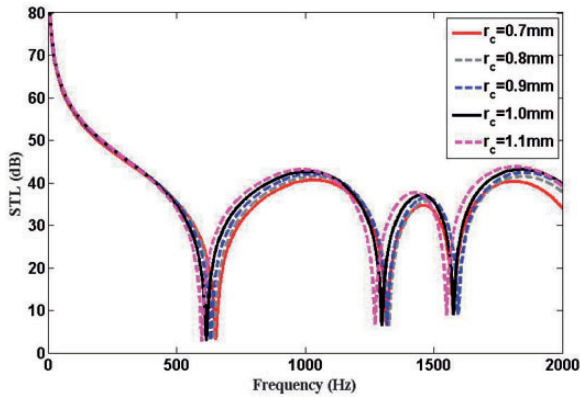
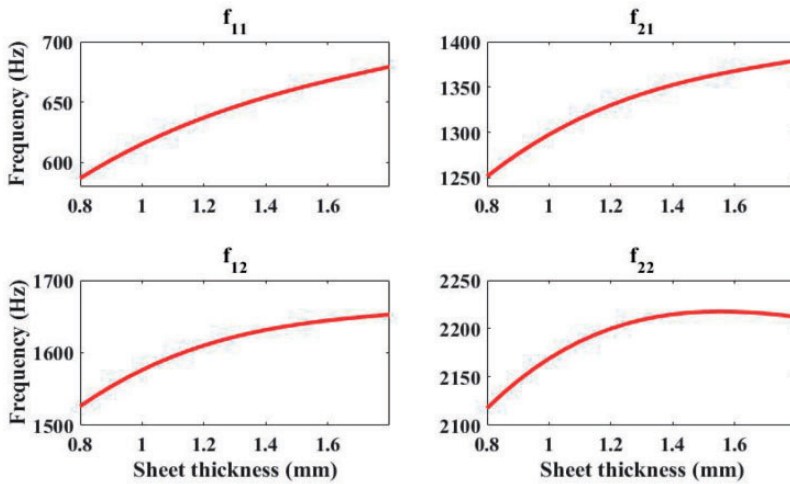**Figure 12.** Effect of rod radius on STL of the sandwich plate.

Figure 13. Effect of the thickness of face sheets on the first four natural frequencies.

overall sound insulation performance could be achieved, because the increased rod radius leads to increased equivalent mass density to help in sound insulation [35]. But a larger rod radius inevitably leads to a larger mass density. Therefore, some compromise is indispensable if light weight and good sound insulation are both demanded. In consequence, the rod radius needs to be chosen rationally in different application situations.

With the increase of the face sheets thickness (i.e., h_f), the mass and effective stiffness of the sandwich plate are both increased. Hence, it is anticipated that the thickness of face sheets must also have great influences on the natural frequencies and STL. From Figure 13, it is observed that the first three natural frequencies
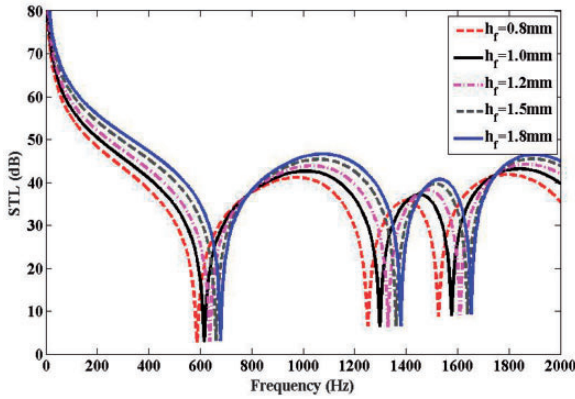
Figure 14. Effect of the thickness of face sheets on STL of the sandwich plate.

increase with the increase of h_f. While h_f increases from 0.8 mm to 1.8 mm, the fourth natural frequency first increases then decreases, which shows a similar trend to that of Guo et al. [49]. This could be explained by combination effects of the effective mass and stiffness: a larger mass results in lower natural frequencies, while a larger stiffness brings about higher natural frequencies. The increase of effective mass dominates in high frequency range while the increase of effective stiffness dominates in low frequency range. The increase of the thickness (i.e., h_f) implies the simultaneous increasing mass and stiffness, therefore, effect on the natural frequencies is nonmonotonic and dependent on whether the mass or the stiffness is in the domination.

Figure 14 shows the STL of sandwich plate for various thicknesses of face sheet when the incident angle $\beta = \pi/6$ and the azimuth angle $\theta = \pi/4$. With the increase of h_f, all the first three sound troughs move to higher frequencies, and the sandwich plate exhibits better STL which is easily understood that larger thickness leads to better sound insulation performance. However, since the increase of h_f counters to the demand for light-weight, a proper h_f should be selected to compromise light-weight and sound insulation.

Effect of the incident angle β of the sound wave on the STL of sandwich plate is investigated by keeping $\theta = \pi/4$. It is observed from Figure 15 that with increase in β, the performance of sound transmission becomes worse in the frequency range from 0 to 1300 Hz and it first gets worse and then better in the higher frequency range, because of the possibility of constructive interference between incident sound wave and structural bending wave in the former [50]. And it can be observed that some sound troughs disappear when the incident angle is 0 due to that the sound wave cannot stimulate all vibration modes of the sandwich plate.

For the given incident angle of $\pi/6$, Figure 16 shows the effect of azimuth angle θ of the sound wave on the STL of sandwich plate. It is found with θ being 0 which
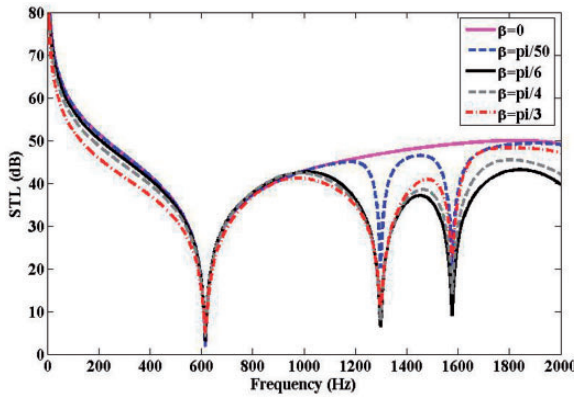
Figure 15. Effect of different incident angles on STL of sandwich plate with azimuth angle $\theta = \pi/4$.
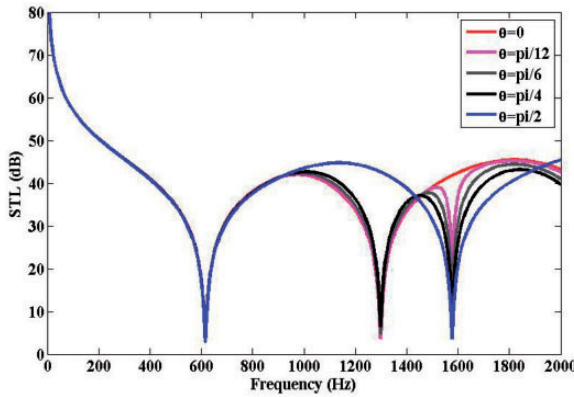

Figure 16. Effect of different azimuth angles on STL of sandwich plate with incident angle $\beta = \pi/6$.

means that the incident wave is parallel to the x-axis, the third sound trough disappears due to the fact that the third-order vibration mode of the rectangle sandwich plate cannot be stimulated by the sound wave. For a similar reason, when θ being $\pi/2$ which indicates that the incident wave becomes parallel to the y-axis, the second trough disappears, because the second-order vibration mode is not able to be stimulated which can be easily understood in Figure 17. Some comments from the point of mathematical view are also provided to give a more in-depth explanation. Take the case of $\theta = 0$ as example and recall that $k_y = k_0 \sin\beta \sin\theta$. The component of the wave number along the y-axis direction is zero, i.e., $k_y = 0$. It implies that for the incident wave, along the direction parallel
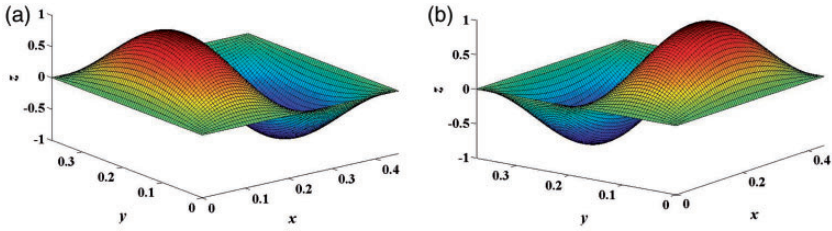
Figure 17. (a) (2, 1) modal shape for $f = 1298$ Hz, (b) (1, 2) mode shape for $f = 1577$ Hz.

to the y-axis, there is no phase difference, i.e., amplitudes of the incident pressure in equation (17) are y-independent

$$P_{imn} = -\frac{4}{na\pi}\int_0^a P_{i0}e^{-jk_x x}\sin\frac{m\pi x}{a}[\cos n\pi - 1]\mathrm{d}x \tag{31}$$

From equation (31), it can be found that when n are even numbers including (1, 2), P_{imn} becomes zero. This gives the mathematical explanation for why some vibration modes cannot be stimulated (i.e., $P_{imn} = 0$) under the excitation of the incident wave with $\theta = 0$. Similarly, following the same procedure, one can rigorously derive the conclusion that the second-order vibration mode (as shown in Figure 17(a)) of the plate cannot be stimulated with $\theta = \pi/2$.

In addition to the above findings, it is noted that in low frequency range there is nearly no variation in the STL through sandwich plate for different azimuth angles. Thus, from the perspective of the behavior in low frequency range, the influence of θ on the STL can be almost ignored.

Effect of material properties

In practice, different components of the sandwich plate are often made of different materials in consideration of its multi-functionalities, and sometimes they perform better than the sandwich structure with a single material in specific properties [35]. Various configurations are considered in this section. For example, S–S–S denotes the sandwich plate with face sheets and core layer made of steel and Al–S–Al denotes the sandwich plate with core layer made of steel and face sheets made of aluminum. In the following case study, the influence of different combinations of steel, Al and Ti materials on sound transmission characteristics is studied. For Al and Ti, the Young's moduli are 77.6 and 107 GPa, respectively; the mass densities are 2730 and 4510 kg/m³, respectively; the Poisson's ratio are 0.35 and 0.32, respectively. Material properties of steel have already been listed in Table 2.

In Figure 18(a), dimensions of the sandwich structure are kept constant and only the variations of the materials are considered. It is noted that the combination of S–Ti–S, S–Al–S have the higher frequency for the first sound trough, and in general, the combination of S–S–S exhibits the best performance in terms of sound
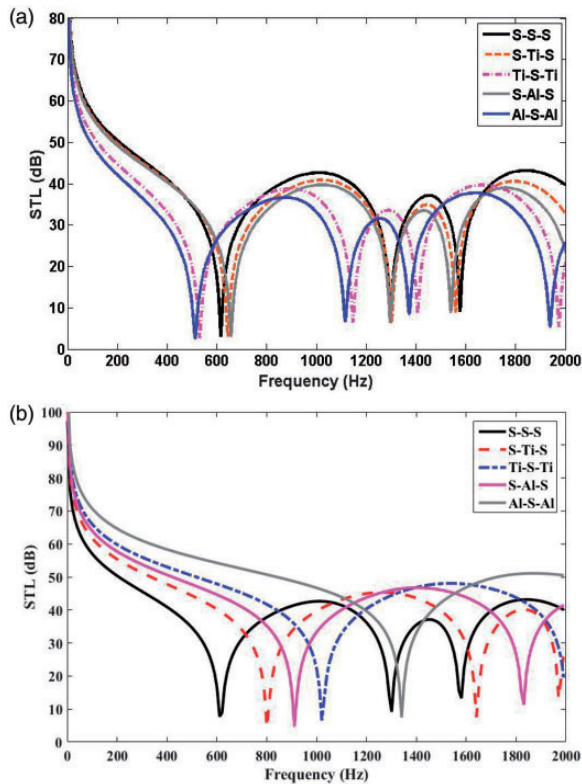
Figure 18. Comparison of the STL for hourglass lattice core sandwich plate with different combination of materials, (a) with same dimensions, (b) with same weight.

insulation in the concerned frequency range of 0–2000 Hz. Without loss of generality, the rules of weight equality are used and the dimensions are kept constant except for h_f, h_c and material properties. It is worth mentioning that the ratio of h_c to h_f is fixed to be 15 to ensure the validity of the modeling theory. Figure 18(b) shows that the combination of Al–S–Al outperforms other combinations in terms of the sound transmission characteristics. The combination of S–S–S shows the worst performance, because of its lowest shear stiffness. In practice, the engineering structures are usually designed to avoid the potential external excitation frequency and/or achieve the proper dimensions and weight. Therefore, different combinations of materials should be carefully designed for the application of the lattice sandwich plates with different purposes.

Conclusions

This article has presented a study on the sound transmission characteristics of sandwich plate with the hourglass lattice truss core. The Reissner sandwich plate

theory has been used to establish the vibro-acoustic coupling model of the lattice sandwich plate. The developed theoretical model is verified by comparing with the existing literature and FEM. A parametric study has been conducted to investigate the effects of structural and material parameters on sound insulation performance of the sandwich plate. It has been found that by appropriately tuning the geometric parameters, the hourglass core sandwich plate can exhibit a better STL performance than traditional lattice core sandwich plates. Moreover, by selecting different combinations of materials, a desirable sound insulation may be achieved. The results of this work provide some guidelines for the design of hourglass lattice core sandwich plate in the applications for sound insulation.

Declaration of Conflicting Interests

The author(s) declared no potential conflicts of interest with respect to the research, authorship, and/or publication of this article.

Funding

ORCID iD

Lihua Tang ⬤ https://orcid.org/0000-0001-9031-4190

References

1. Zhang J, Supernak P, Mueller-Alander S, et al. Improving the bending strength and energy absorption of corrugated sandwich composite structure. *Mater Des* 2013; 52: 767–773.
2. Ebrahimi H, Ghosh R, Mahdi E, et al. Honeycomb sandwich panels subjected to combined shock and projectile impact. *Int J Impact Eng* 2016; 95: 1–11.
3. Zhao X, Zhang B and Li YM. Vibration and acoustic radiation of an orthotropic composite cylindrical shell in a hygroscopic environment. *J Vib Control* 2017; 23: 673–692.
4. Ruzzene M. Vibration and sound radiation of sandwich beams with honeycomb truss core. *J Sound Vib* 2004; 277: 741–763.
5. Moosavimehr SE and Phani AS. Sound transmission loss characteristics of sandwich panels with a truss lattice core. *J Acoust Soc Am* 2017; 141: 2921.
6. Bollen P, Quievy N, Detrembleur C, et al. Processing of a new class of multifunctional hybrid for electromagnetic absorption based on a foam filled honeycomb. *Mater Des* 2016; 89: 323–334.
7. Roper CS. Multiobjective optimization for design of multifunctional sandwich panel heat pipes with micro-architected truss cores. *Int J Heat Fluid Flow* 2011; 32: 239–248.
8. Kim T, Hodson HP and Lu TJ. Fluid-flow and endwall heat-transfer characteristics of an ultralight lattice-frame material. *Int J Heat Mass Transfer* 2004; 47: 1129–1140.

9. Fan HL and Fang DN. Enhancement of mechanical properties of hollow-strut foams: analysis. *Mater Des* 2009; 30: 1659–1666.
10. Davalos JF, Qiao PZ, Ramayanam V, et al. Torsion of honeycomb FRP sandwich beams with a sinusoidal core configuration. *Compos Struct* 2009; 88: 97–111.
11. Morada G, Vadean A and Boukhili R. Failure mechanisms of a sandwich beam with an ATH/epoxy core under static and dynamic three-point bending. *Compos Struct* 2017; 176: 281–293.
12. Yang W, Xiong J, Feng LJ, et al. Fabrication and mechanical properties of three-dimensional enhanced lattice truss sandwich structures. *J Sandw Struct Mater*. Epub ahead of print 24 July 2018. DOI: 10.1177/1099636218789602
13. Simsek M and Al-Shujairi M. Static, free and forced vibration of functionally graded (FG) sandwich beams excited by two successive moving harmonic loads. *Composites Part B* 2017; 108: 18–34.
14. Filippi M and Carrera E. Bending and vibrations analyses of laminated beams by using a zig-zag-layer-wise theory. *Composites Part B* 2016; 98: 269–280.
15. Aguib S, Nour A, Zahloul H, et al. Dynamic behavior analysis of a magnetorheological elastomer sandwich plate. *Int J Mech Sci* 2014; 87: 118–136.
16. Baba BO. Free vibration analysis of curved sandwich beams with face/core debond using theory and experiment. *Mech Adv Mater Struct* 2012; 19: 350–359.
17. Li S, Yang JS, Wu LZ, et al. Vibration behavior of metallic sandwich panels with hourglass truss cores. *Mar Struct* 2019; 63: 84–98.
18. Cotoni V, Shorter P and Langley R. Numerical and experimental validation of a hybrid finite element-statistical energy analysis method. *J Acoust Soc Am* 2007; 122: 259–270.
19. Yin H, Yu DJ, Lv H, et al. Hybrid finite element/statistical energy method for mid-frequency analysis of structure-acoustic systems with interval parameters. *J Sound Vib* 2015; 353: 181–204.
20. Hynna P, Klinge P and Vuoksinen J. Prediction of structure-borne sound-transmission in large welded ship structures using statistical energy analysis. *J Sound Vib* 1995; 180: 583–607.
21. Craik RJM, Nightingale TRT and Steel JA. Sound transmission through a double leaf partition with edge flanking. *J Acoust Soc Am* 1997; 101: 964–969.
22. Ghinet S and Atalla N. The transmission loss of curved laminates and sandwich composite panels. *J Acoust Soc Am* 2005; 118: 774–790.
23. Lee JH and Kim J. Analysis of sound transmission through periodically stiffened panels by space-harmonic expansion method. *J Sound Vib* 2002; 251: 349–366.
24. Lee JH and Kim J. Sound transmission through periodically stiffened cylindrical shells. *J Sound Vib* 2002; 251: 431–456.
25. Wang J, Lu TJ, Woodhouse J, et al. Sound transmission through lightweight double-leaf partitions: theoretical modelling. *J Sound Vib* 2005; 286: 817–847.
26. Xin FX and Lu TJ. Transmission loss of orthogonally rib-stiffened double-panel structures with cavity absorption. *J Acoust Soc Am* 2011; 129: 1919–1934.
27. Wang DW, Ma L, Wang XT, et al. Sound transmission loss of sandwich plate with pyramidal truss cores. *J Sandw Struct Mater*. Epub ahead of print 26 February 2018. DOI: 10.1177/1099636218759683
28. Maxit L. Wavenumber space and physical space responses of a periodically ribbed plate to a point drive: a discrete approach. *Appl Acoust* 2009; 70: 563–578.

29. Lauriks W, Mees P and Allard JF. The acoustic transmission through layered systems. *J Sound Vib* 1992; 155: 125–132.
30. Pellicier A and Trompette N. A review of analytical methods, based on the wave approach, to compute partitions transmission loss. *Appl Acoust* 2007; 68: 1192–1212.
31. El-Raheb M and Wagner P. Effects of end cap and aspect ratio on transmission of sound across a truss-like periodic double panel. *J Sound Vib* 2002; 250: 299–322.
32. Yang Y, Mace BR and Kingan MJ. Prediction of sound transmission through, and radiation from, panels using a wave and finite element method. *J Acoust Soc Am* 2017; 141: 2452–2460.
33. Xin FX, Lu TJ and Chen AQ. Sound transmission through simply supported finite double-Panel partitions with enclosed air cavity. *J Vib Acoust Trans ASME* 2010; 132: 011008.
34. Fu T, Chen ZB, Yu HY, et al. Sound transmission loss behavior of sandwich panel with different truss cores under external mean airflow. *Aerosp Sci Technol* 2019; 86: 714–723.
35. Liu J, Chen TT, Zhang YH, et al. On sound insulation of pyramidal lattice sandwich structure. *Compos Struct* 2019; 208: 385–394.
36. Carneal JP and Fuller CR. An analytical and experimental investigation of active structural acoustic control of noise transmission through double panel system. *J Sound Vib* 2004; 272: 749–771.
37. Feng LJ, Wu LZ and Yu GC. An hourglass truss lattice structure and its mechanical performances. *Mater Des* 2016; 99: 581–591.
38. Feng LJ, Xiong J, Yang LH, et al. Shear and bending performance of new type enhanced lattice truss structures. *Int J Mech Sci* 2017; 134: 589–598.
39. Wei K, Yang QD, Yang XJ, et al. Mechanical analysis and modeling of metallic lattice sandwich additively fabricated by selective laser melting. *Thin Walled Struct* 2020; 146: 106189. DOI: 10.1016/j.tws.2019.106189
40. Speare PR and Kemp KO. A simplified Reissner theory for plate bending. *Int J Solids Struct* 1977; 13: 1073–1079.
41. Deshpande VS and Fleck NA. Collapse of truss core sandwich beams in 3-point bending. *Int J Solids Struct* 2001; 38: 6275–6305.
42. Allen HG. *Analysis and design of structural sandwich panels*. Oxford: Pergamon, 1969.
43. Lou J, Ma L and Wu LZ. Free vibration analysis of simply supported sandwich beams with lattice truss core. *Mater Sci Eng B* 2012; 177: 1712–1716.
44. Yang XD, Guo ZK, Zhang W, et al. Substitution method: a technique to study dynamics of both non-gyroscopic and gyroscopic systems. *J Sound Vib* 2019; 458: 510–521.
45. Guo ZK, Liu CC and Li FM. Vibration analysis of sandwich plates with lattice truss core. *Mech Adv Mater Struct* 2019; 26: 424–429.
46. Chen JW, Liu W and Su XY. Vibration and buckling of truss core sandwich plates on an elastic foundation subjected to biaxial in-plane loads. *Comp Mater Continua* 2011; 24: 163–181.
47. Li XY, Yu KP, Zhao R, et al. Sound transmission loss of composite and sandwich panels in thermal environment. *Composites Part B* 2018; 133: 1–14.
48. Li M, Li FM and Jing XJ. Active vibration control of composite pyramidal lattice truss core sandwich plates. *J Aerosp Eng* 2018; 31: 04017097.
49. Guo ZK, Yang XD and Zhang W. Dynamic analysis, active and passive vibration control of double-layer hourglass lattice truss structures. *J Sandw Struct Mater*. Epub ahead of print 27 June 2018. DOI: 10.1177/1099636218784339

50. Xin FX and Lu TJ. Analytical modeling of fluid loaded orthogonally rib-stiffened sandwich structures: sound transmission. *J Mech Phys Solids* 2010; 58: 1374–1396.

Appendix 1

Figure 19 shows the deformation diagram of the simply supported sandwich plate. It is assumed that there exists an in-plane rotating angle φ_y for the core layer on the planes $x = 0$ (*a*), while there is no rotation for the face sheets, which forms a discontinuity between them. But in fact, the face sheets should be continuous with the core layer which indicates φ_y has to be 0, due to that the displacements of four sides of the sandwich plate are all zero under the simply supported boundary conditions. The premise of this assumption is that the core layer can be regarded as very soft and only has very minor contribution to the bending stiffness of sandwich plate [48]. Similarly, φ_x should be 0 on the planes $y = 0$ (*b*) for the simply supported sandwich plate.
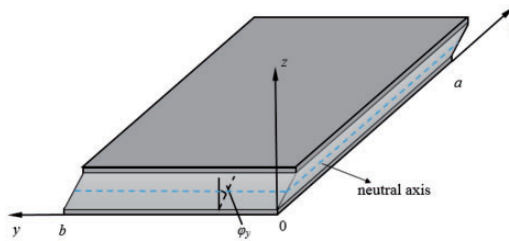

Figure 19. Deformation diagram of a differential element of the sandwich plate.

Appendix 2

The simply supported boundary conditions are given in equation (5). Substituting equation (5) into equation (1) yields

$$w = 0, \qquad \frac{\partial \varphi_x}{\partial x} = 0, \qquad \varphi_y = 0 \tag{32}$$

Substituting equation (3) into equation (32), one obtains

$$\psi - \frac{D}{C}\nabla^2\psi = 0, \qquad \frac{\partial^2\psi}{\partial x^2} + \frac{\partial^2 f}{\partial x\partial y} = 0, \qquad \frac{\partial\psi}{\partial y} - \frac{\partial f}{\partial x} = 0 \tag{33}$$

And equation (33) can be simplified as

$$\psi = 0, \qquad \nabla^2\psi = 0, \qquad \frac{\partial f}{\partial x} = 0 \tag{34}$$

From equations (4) and (34), f should be 0 for simply supported boundary conditions.

Appendix 3

The supplementary study is provided to prove the bending stiffness of core layer is reasonably to be neglected if the structural parameters change within certain ranges. The equivalent elastic modulus of core layer is given in Deshpande and Fleck [41] as $E_c = E_f \bar{\rho} \sin^4 \alpha$. Thus, the bending stiffness of core layer is obtained to be $D_c = \frac{E_c h_c^3}{12(1-\nu_f^2)}$. For different r_c, h_f, and h_c, the effective bending stiffnesses of the sandwich plates with and without the cores are given in Tables 4 to 6. The other material and structural parameters used in the calculation are the same as those in "Comparison of different lattice cores" section. It can be seen that the bending stiffness of core layer can be relatively neglected as compared to total bending stiffness of the sandwich plate for certain structural sizes.

Table 4. Effects of rod radius on bending stiffness of the sandwich plate.

r_c (mm)	0.7	0.8	0.9	1.0	1.1
D (without core, Pa·m³)	29,538	29,538	29,538	29,538	29,538
$D + D_c$ (with core, Pa·m³)	30,166	30,358	30,576	30,820	31,089
Relative errors(%)	−2.0	−2.7	−3.4	−4.2	−5.0

Table 5. Effects of face sheet thickness on the bending stiffness of the sandwich plate.

h_f (mm)	0.8	1.0	1.2	1.5	1.8
D (without core, Pa·m³)	23,043	29,538	36,338	47,120	58,619
$D + D_c$ (with core, Pa·m³)	24,325	30,820	37,619	48,402	59,900
Relative errors(%)	−5.3	−4.2	−3.4	−2.9	−2.1

Table 6. Effects of height of the core layer on bending stiffness of the sandwich plate.

h_c (mm)	7	9	11	13	15
D (without core, Pa·m³)	7385	11,538	16,615	22,615	29,538
$D + D_c$ (with core, Pa·m³)	7412	11,645	16,911	23,278	30,820
Relative errors(%)	−0.4	−0.9	−1.8	−2.8	−4.2